The Antarctic Circumpolar Wave in a Coupled Ocean–Atmosphere GCM

M. CHRISTOPH

Max Planck Institute for Meteorology, Hamburg, Germany

T. P. BARNETT

Scripps Institution of Oceanography, University of California, San Diego, La Jolla, California

E. ROECKNER

Max Planck Institute for Meteorology, Hamburg, Germany

(Manuscript received 8 April 1997, in final form 12 September 1997)

ABSTRACT

A phenomenon called the Antarctic Circumpolar Wave (ACW), suggested earlier from fragmentary observational evidence, has been simulated realistically in an extended integration of a Max Planck Institute coupled general circulation model. The ACW both in the observations and in the model constitutes a mode of the coupled ocean–atmosphere–sea-ice system that inhabits the high latitudes of the Southern Hemisphere. It is characterized by anomalies of such climate variables as sea surface temperature, sea level pressure, meridional wind, and sea ice that exhibit intricate and evolving spatial phase relations to each other.

The simulated ACW signal in the ocean propagates eastward over most of the high-latitude Southern Ocean, mainly advected along in the Antarctic Circumpolar Current. On average, it completes a circuit entirely around the Southern Ocean but is strongly dissipated in the South Atlantic and in the southern Indian Ocean, just marginally maintaining statistical significance in these areas until it reaches the South Pacific where it is reenergized. In extreme cases, the complete circumpolar propagation is more clear, requiring about 12–16 yr to complete the circuit. This, coupled with the dominant zonal wavenumber 3 pattern of the ACW, results in the local reappearance of energy peaks about every 4–5 yr.

The oceanic component of the mode is forced by the atmosphere via fluxes of heat. The overlying atmosphere establishes patterns of sea level pressure that mainly consist of a standing wave and are associated with the Pacific–South American (PSA) oscillation described in earlier works. The PSA, like its counterpart in the North Pacific, appears to be a natural mode of the high southern latitudes. There is some ENSO-related signal in the ACW forced by anomalous latent heat release associated with precipitation anomalies in the central and western tropical Pacific. However, ENSO-related forcing explains at most 30% of the ACW variance and, generally, much less.

It is hypothesized that the ACW as an entity represents the net result of moving oceanic climate anomalies interacting with a spatially fixed atmospheric forcing pattern. As the SST moves into and out of phase with the resonant background pattern it is selectively amplified or dissipated, an idea supported by several independent analyses. A simplified ocean heat budget model seems to also support this idea.

1. Introduction and background

The existence of the so-called Antarctic Circumpolar Wave (ACW) has recently been postulated from observations (White and Peterson 1996, hereafter WP). These authors note this ''wave'' is manifest by an eastward propagating signal in both ocean and atmospheric variables of the high southern latitudes. Phase-locked signals in the sea surface temperature (SST), sea level pressure (SLP), meridional wind stress (MWS), and sea-ice extent (SIE) were seen to apparently propagate around the Antarctic continent in about 8–10 yr. At any one location, this signal appears to repeat itself in about 4–5 yr.

In view of the very short observational records in the data-sparse region available for the first description of the ACW, it will come as a surprise to many that the phenomenon has been simulated, much as described by White and Peterson, in a long control integration of a coupled general circulation model (CGCM) of the Max-Planck Institute for Meteorology and the German Climate Computing Center (Hamburg). The appearance and properties of the ACW in this simulation are described in section 2 by various analysis methods and

Corresponding author address: Dr. Michael Christoph, Max-Planck-Institut für Meteorologie, Bundesstraße 55, D-20146 Hamburg, Germany.
E-mail: christoph@dkrz.de

are also compared to the description offered by WP. The physical processes that generate and maintain the feature are studied in section 3.

The climate model that produced the results for this study contains a T42 resolution atmospheric model [ECHAM4, Roeckner et al. (1996)]. T42 corresponds to a spatial grid of approximately 2.8° × 2.8°. This model has 19 levels in the vertical and a host of modern physical parameterizations. Also included in the coupled model is the OPYC3 ocean model operated at the same spatial resolution outside the Tropics as was the atmospheric model, but with much higher resolution in the equatorial region to resolve El Niño–Southern Oscillation (ENSO) physics (Oberhuber 1993a,b). This ocean model is posed in isopycnal coordinates with an embedded mixed layer and a dynamical sea ice model including viscous-plastic rheology. An annual flux correction of heat and freshwater is applied to maintain the mean state of the model near that observed. However, the annual cycle evolves freely with no correction (Bacher et al. 1996). The model also reproduces the strength of the ENSO signal realistically in both the ocean and the atmosphere of the Tropics and, importantly, the midlatitudes, with two caveats. The ENSO signal in the CGCM has energy in a broad band from 2 to 5 yr, but the majority of events occur at slightly too high a frequency (27 months). It is also true that the events are too locally confined about the equator (Bacher et al. 1996; Roeckner et al. 1996), a feature common to most CGCMs.

2. Description of the ACW

We analyzed 180 yr of the control CGCM run for which no specific model design or parameter setting had been employed; that is, the model was in no way tuned to produce the ACW. Monthly time series of SST, MWS, SLP, SIE, as well as sea level, mixed layer depth, horizontal ocean currents, heat fluxes, and total precipitation were extracted for analysis. After removal of the seasonal cycle, the data were run through a bandpass filter with half-power points of 1 and 20 yr, respectively, in order to suppress noise and ultra-low-frequency variability. Filter weights were calculated with the help of cubic splines (A. Bacher 1995, personal communication), which resulted in a filter response whose cutoff slopes were somewhat steeper than those from a corresponding Gaussian filter. Prior to the application of an extended empirical orthogonal function (EEOF) analysis (Weare and Nasstrom 1982) and composite techniques (section 3), the time series were further smoothed by forming 6-month averages for purposes of better handling the large data amounts.

Our first task was to compute the same quantities from the CGCM data as shown by WP in order to compare them. We first calculated time–longitude diagrams of bandpass-filtered anomalies for SST, SLP, and MWS (Fig. 1) averaged meridionally between 54° and 63°S. For the sake of conciseness, only the first 30 yr are displayed here. Clear patterns of dominating eastward propagation are visible for SST, moving at an average phase speed of 0.04–0.06 m s^{-1} (vs 0.06–0.08 m s^{-1} observed). In contrast to the findings of WP, the patterns for SLP and MWS seem to be governed mainly by standing oscillations. Note that in accordance with observations, the most intense model ACW anomalies are found in the Pacific sector and the ranges are as large as 0.5 K in SST, 4 hPa in SLP, and 0.02 Pa in MWS, which are values comparable in magnitude with those found by WP.

We next estimated the two-dimensional wavenumber-frequency spectrum of the unfiltered SST around 57°S. Our spectral estimates typically each have at least 40 realizations, as opposed to the single realization in the WP analysis, and so are statistically robust. The results (Fig. 2), which can be compared with WP's (Fig. 1, lower), show the predominance of both wavenumbers 2 and 3 for eastward propagation in the SST and a peak power at periods of about 4 yr. There was no significant power for westward propagation, and, therefore, no plot is shown. The frequency of the spectral peak(s) is in agreement with WP's result. However, they found a characteristic wavenumber of 2, whereas our results show both wavenumbers 2 and 3. In the model, about 20% of the realizations clearly looked like the observed wavenumber 2 feature and propagated at the same rate as in the observations. The model suggests there is considerable variability in both the time and space scales of the ACW from realization to realization. This makes it difficult to compare the WP analysis of a single event with the CGCM and to then comment on model validity.

The temporal phase relationship between two ACW components at the same location is illustrated in Fig. 3 by means of lagged cross correlations. For that purpose, bandpass filtered fields were averaged over the latitudes 54°–63°S and zonal averages of cross-correlation curves between two quantities were formed. Here, correlation values larger than 0.21 are necessary for confidence at the 95% level. It is shown that SST is almost 90° out of phase with SLP, that is, low (high) SLPs are followed by cold (warm) SSTs about 1 yr later, and almost 180° out of phase with MWS or SIE; that is, warm (cold) SSTs are associated with southerly (northerly) winds and a retreat (extension) of sea ice. Correlating SST with the net surface heat flux reveals a 90° out-of-phase relationship, which is indicative of upward (downward) heat fluxes preceding cold (warm) SSTs by 1 yr.

Next we carried out an EEOF analysis of SST (Fig. 4) and directly compared our results with WP (their Fig. 4) in order to confirm that there is eastward propagation in this field. The results clearly show such propagation and suggest a circumpolar transit time of 12–16 yr, compared to the 8–10 yr obtained by WP. The evolution of time–space relationships between SST and other ACW components was investigated by means of combined EEOFs of SST together with variables described at the

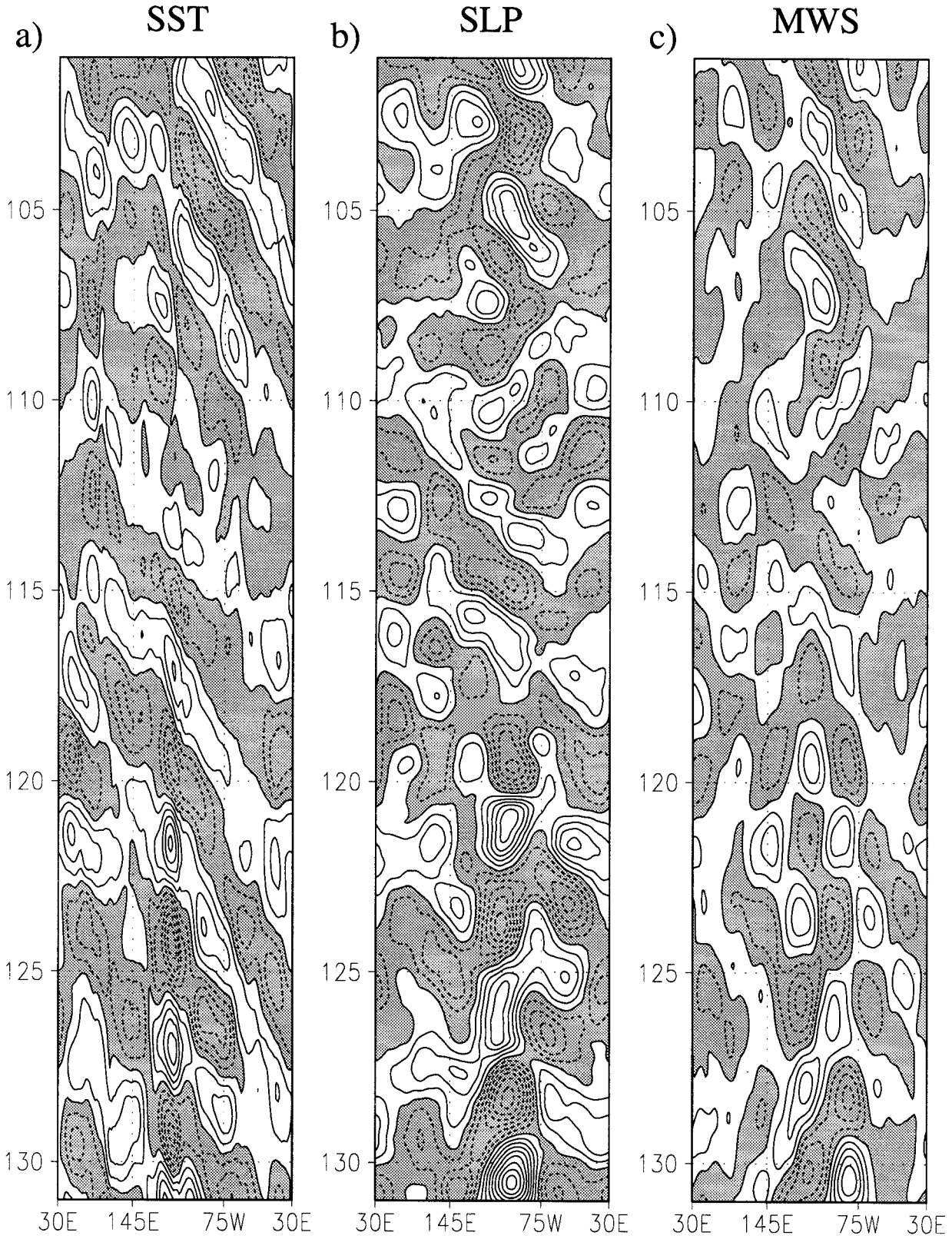

FIG. 1. Hovmoeller diagrams of anomalies (averaged over latitudes 54°–63°S) (a) in SST, (b) SLP, and (c) MWS for model years 101–130. Negative and southward anomalies are shaded. Contour intervals are 0.1 K for SST, 0.5 hPa for SLP, and 0.005 Pa for MWS.

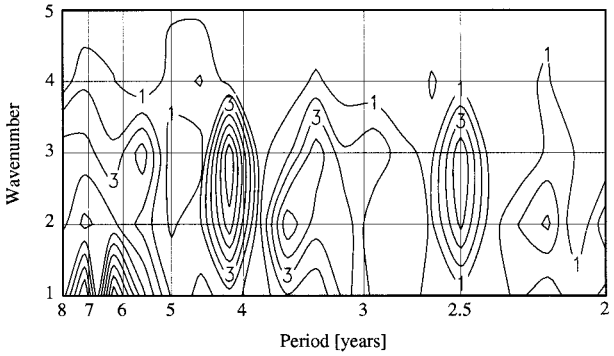

FIG. 2. Wavenumber-frequency spectrum along 57°S for eastward propagation computed from unfiltered monthly mean SST data. Contour interval is 10^{-3} K^2 month^{-1}.

beginning of this section (no figures shown). It turns out that phase-locked signals only in SST and SIE do in fact propagate. The associated atmospheric anomaly patterns remain geographically rather fixed. The spatial relationship among atmospheric variables is such that, for instance, high (low) pressure anomalies are found about 20° downstream of downward (upward) heat fluxes and northerly (southerly) wind anomalies about 30° upstream of high (low) pressures.

A simplified schematic of the relation among the SST, SLP, MWS, and net surface heat flux was constructed (Fig. 5) for a specific phase of the ACW that summarizes the results made so far. The general structure of the schematic was similar in many ways to the one drawn by WP (their Fig. 3), but there were some critical differences. (i) As mentioned earlier the CGCM distinctly favored, although not exclusively, a wavenumber 3 distribution of all ACW components around the Antarctic continent. (ii) Another important difference was that the

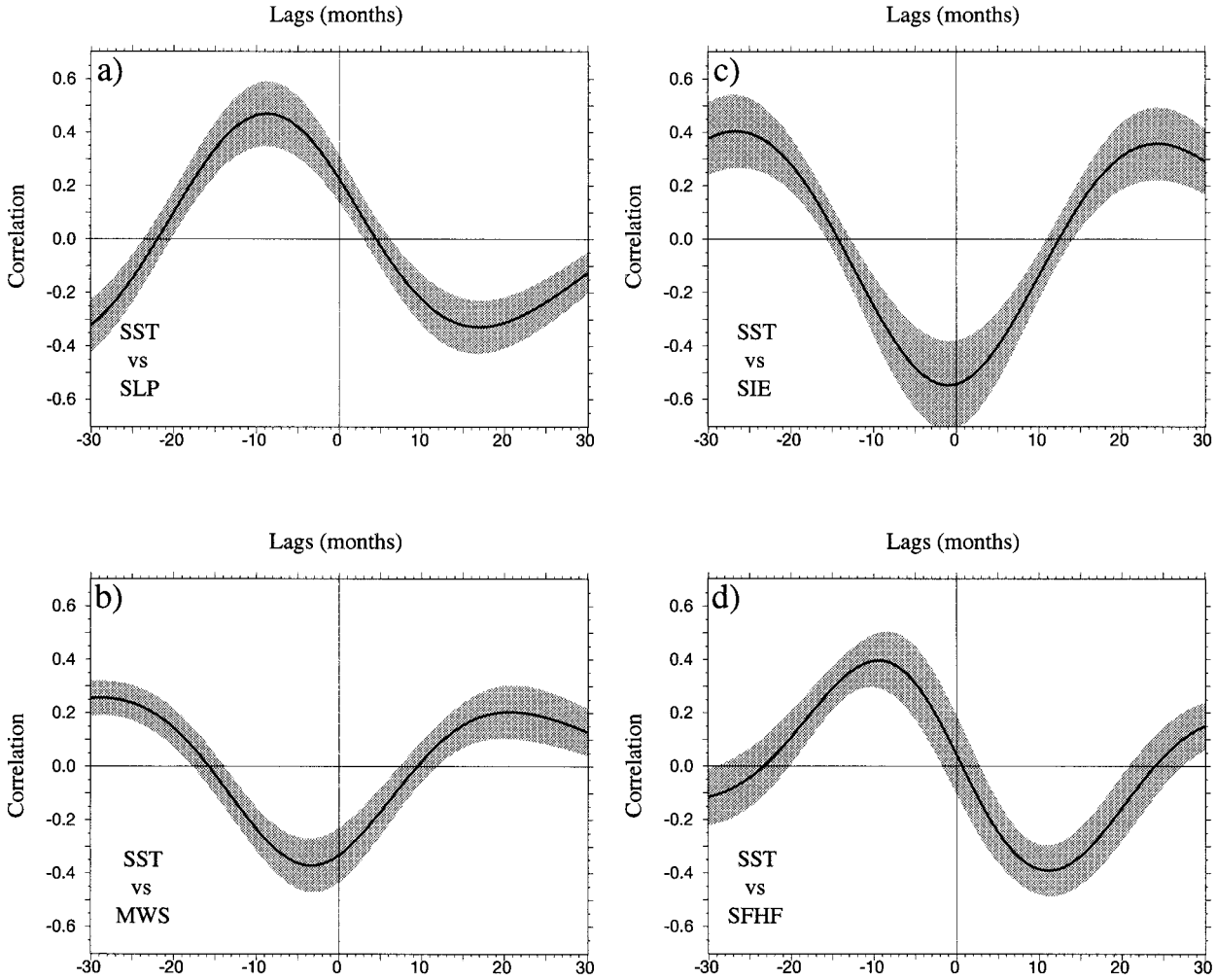

FIG. 3. Zonal mean of lagged cross correlations between the indicated quantities, averaged over latitudes 54°–63°S. Positive lags indicate the first quantity leading the second, and vice versa for negative lags. Shading denotes the variability of correlation curves at individual longitudes as measured by the standard deviation.

WP composite suggests the amplitude of the ACW is about the same at both of its local maxima. In our case, the magnitude of the local maximum in the South Atlantic and south Indian Oceans is much weaker than found in the Pacific. In fact, it is so weak, that it raises a serious question as to whether or not the features of the ACW do indeed propagate around the entire Antarctic continent as indicated by the EEOF analysis. An equally plausible description would have the ACW being apparent first south of Australia, subsequently moving eastward and intensifying. After being squeezed through the Drake Passage, the signal begins to rapidly attenuate, with little or no remnant remaining by the time it reaches the tip of Africa. We shall investigate this possibility further in the next section. (iii) While the SST and sea-ice components of the ACW appear to propagate, the SLP, MWS, and net surface heat flux are more closely similar to standing waves.

3. Physics of the ACW

The longer and more complete CGCM datasets allow us to investigate, quantitatively, the origins of the ACW, at least as it is produced in the model. We posed these studies as a series of questions, first regarding the local properties and maintenance of the ACW and then regarding the mechanism by which it is generated in the first place.

a. How is the ACW locally generated?

The ACW is a mode of the coupled ocean–atmosphere–sea-ice system. In order to find out which part of the system drove the mode locally, we investigated the heat budget of the ocean's mixed layer. Figure 5 shows a specific phase of the ACW where the maxima in the net air–sea flux are spatially out of phase with the SST patterns themselves. The sense of the physics is, for example, that the heat flux is warming the eastern margins of the warm anomalies and cooling their western margins (note that positive heat flux is directed downward and negative flux is directed upward). The most influential term in this process is the latent heat flux, which is temporally in phase with the SST tendency at the same location. Further analysis showed the SIE responded to the warmer/colder SST and MWS in just the relation suggested by WP. So far, we have found no indication for SIE playing a driving role in the ACW mechanism. Hence, we will ignore it in the rest of the study. The maintenance of the atmospheric element of the ACW is discussed below.

b. How do the SST anomalies move?

White and Peterson hypothesize that the SST anomalies are simply advected intact by the Antarctic Circumpolar Current (ACC). In the CGCM simulation, the SST anomalies move at 0.04–0.06 m s^{-1} (vs 0.06–0.08 m s^{-1} in WP), while the zonal average strength of the ACC at 55°S, roughly the axis of the ACW, is 0.041 m s^{-1}. Between 150°E and 100°W, the region where the ACW is most energetic, the average ACC speed is 0.047 m s^{-1} in the model. These crude estimates indicate that the eastward currents and the phase speed of the SST anomalies are nearly the same. A more detailed picture of the model's ACC is given by the distribution of the zonal surface velocities shown in the top panel of Fig. 4. Shaded areas clearly mark the climatological position of the ACC whose distinct meanders seem to guide the SST anomalies drawn in the lower panels. Despite these similarities with observations (see WP) there are at least two factors that may lead to somewhat slower than observed surface velocities. First, the simulated mass transport of the ACC based on the Drake Passage throughflow of 120 Sv is perhaps slightly underestimated [direct measurements are of the order 130 Sv according to Read and Pollard (1993)], and second, the ocean model can resolve the surface currents only as the integral over the mixed layer.

In short, the CGCM results appear to support the original hypothesis that the SST anomalies are simply carried by background mean current. However, a far simpler model, described below, will show that there exists another influencing factor.

c. Does the ACW propagate entirely around the Antarctic continent?

The EEOF analysis performed here and by WP suggests this to be the case. However, in our study, we were concerned this could be a figment of the analysis method. Hence, we decided to do a cross-check and resorted to composite analysis of the original, smoothed data to answer this question. The composite's reference times were keyed to both the largest maxima of the first principal components connected with the first EEOF mode of SST displayed in Fig. 4 (the threshold being one standard deviation) and, in a separate analysis, to the maxima of an index of SST at the most energetic region of the ACW (55°S, 120°W). We also estimated the lagged composites relative to the reference times as defined above. The standard deviation between individual realizations of the composite was used in a *t* test to determine the 0.05 significance of the average composite (for details see Barnett 1988). The results for the SST and SLP composites are shown in Figs. 6 and 7, respectively. There appears to be a marginally significant signal in the SST field (Fig. 6) that does propagate around the Antarctic continent near 55°S. The signature of this signal is especially weak in the South Atlantic and southern Indian Oceans, although it can still be faintly discerned. However, the associated signal in the SLP field (Fig. 7) does not show the propagation seen in the SST field. The same may be said for the associated signals in the net heat flux and meridional wind stress fields (not shown).

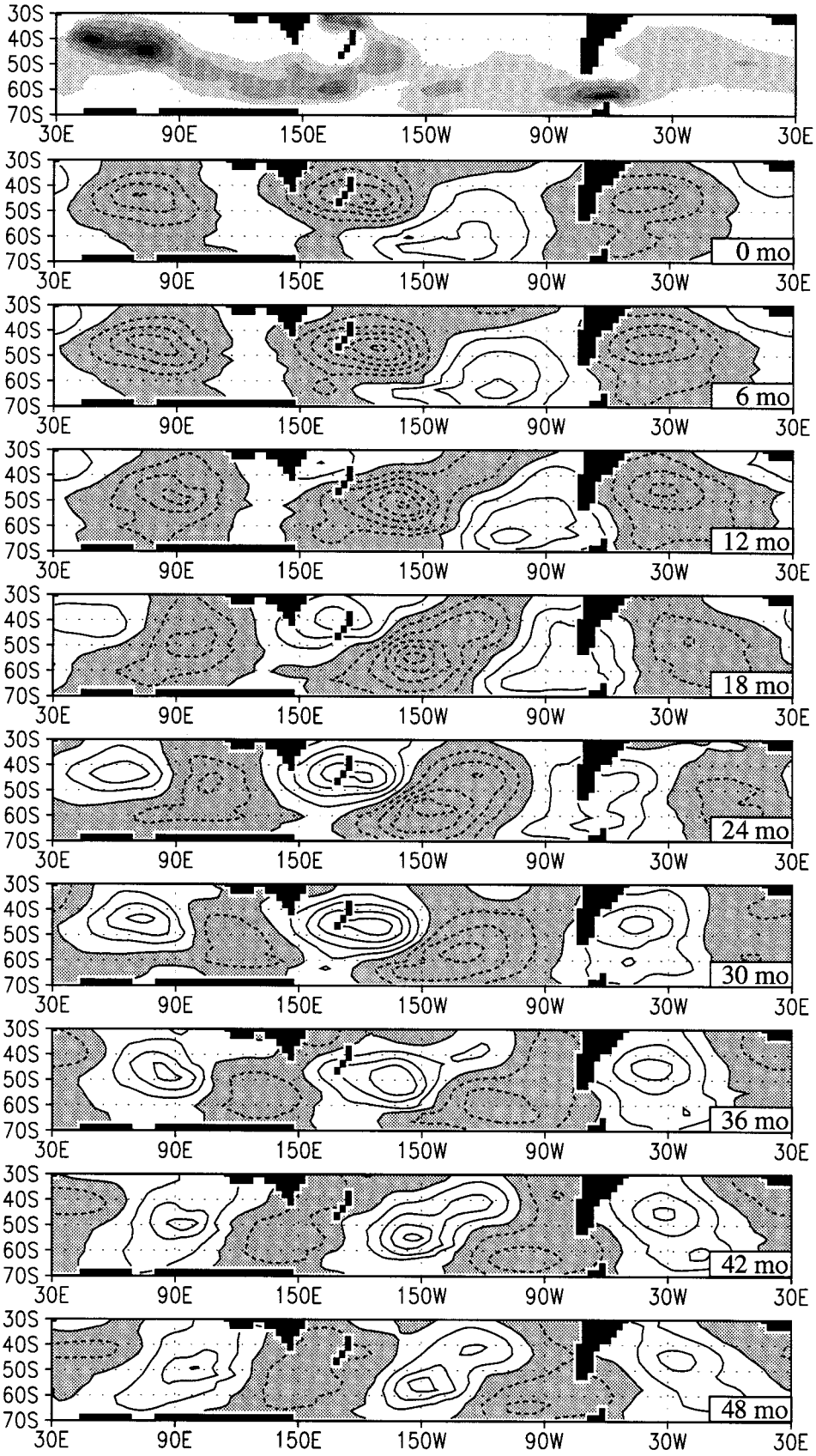

In summary, the simplest analysis of the original CGCM data does marginally support the idea that the ACW signal in the SST field propagates around the entire Antarctic continent, but not the SLP and heat flux fields. The most robust part of the signal is generally first evident south of Australia, moves eastward while intensifying, and then greatly dissipates after it enters the Atlantic Ocean through the Drake Passage. The region of intensification is the region where the air–sea heat exchange directly forces the oceanic component of the ACW as described above. It is also consistent with intuition, which suggests that an SST anomaly, once created by the atmosphere, would have a difficult time maintaining itself without continued forcing in the highly diffusive environment of the ACC, for example, in the South Atlantic and southern Indian Oceans. Nevertheless, it is still remarkable that there exists a climatic feature that can maintain its integrity for years while propagating over such distance.

d. What is the source of the ACW?

White and Peterson speculate that the ACW may have its origins in the ENSO phenomenon. Indeed, the distribution of SLP associated with the ACW (Fig. 7) is similar to the so-called Pacific–South American (PSA) pattern (Mo and White 1985; Karoly 1989). The PSA is essentially the counterpart of the Pacific–North American (PNA) pattern (Horel and Wallace 1981), a much studied feature of the North Pacific region, and one known to be excited by ENSO events (among other factors). If the analogy holds, then the PSA ought to be driven by the release of latent heat associated with ENSO-related anomalous precipitation in the central equatorial Pacific. We constructed regression models to estimate the amount of ACW variance associated with tropical rainfall in the Indo–Pacific region. Empirically, we found that the most influential precipitation region is located in the western and central Pacific (0°–10°N, 180°–120°W), that is, roughly in the region of the major ENSO signal (Fig. 8, top). However, computation of the ''skill'' of the linear regression model according to the equations following below (here expectation values are represented by $\langle\ \rangle$, r denotes the correlation coefficient, y the SLP field, a the field of regression coefficients, and x the index time series of precipitation),

$$\text{Skill} = 100r^2 = 100\left(1 - \frac{\langle \delta^2 y\rangle}{\langle y^2\rangle}\right),$$

with

$$\delta y = y - \hat{y} \quad \text{and} \quad \hat{y} = ax,$$

reveals that the tropical precipitation explained at most 30% of the SLP variance in a region just west of the Drake Passage (Fig. 8, bottom) and less than 10% of the SLP variance over the rest of the ACW domain. We conclude that, while the ENSO signal contributes to the ACW locally, it does not in the CGCM excite the typical atmospheric mode shown in Fig. 7. If this was the case we would expect significant variance contributions also in the remaining parts of the southern midlatitudes. When regressing Niño3 SSTs instead of precipitation the above results did not change notably.

Further proof of the subordinate role of ENSO in the CGCM's ACW is given by the composite study of SST in Fig. 6, which also shows the tropical oceans. It is obvious that on the average peak activity in the Niño3 region occurs every 2–2.5 yr and, thus, differs from the 4–5-yr period of the ACW signal. A bispectrum analysis (Barnett 1991) excluded the possibility of the ACW timescale being a harmonic of the ENSO timescale.

The above suggests the model ACW has its origins in the mid- to high latitudes themselves. The mechanisms that generate and cause the ACW to move have largely been described above. We hypothesize there is one more critical element to the ACW. Prior studies show the strong preference for a zonal wavenumber 3 distribution of SLP in the high latitudes of the Southern Hemisphere (e.g., Mo and White 1985); a distribution that is surprisingly fixed to rather specific geographic locations. The CGCM shows this distribution to be an important part of the ACW (e.g., Fig. 7). We suggest that the moving patterns described above propagate through near-resonant regions of physical space where the wavenumber 3 pattern is preferred. As the resonance kicks in, the ACW signal in the SST, SIE, etc. is strongly amplified, for example, over much of the Western Hemisphere. As the oceanic components move out of resonance with the dominating atmospheric wavenumber 3 pattern, their signals are attenuated/dissipated, for example, in the Eastern Hemisphere. Why is the response not more evident in one of the nodal regions of SLP in the South Atlantic? Perhaps because the response of the CGCM in the South Atlantic is weaker than climatology and that too may be a reason the signals in this region are weak.

e. Can a simple model represent the ACW?

An ocean heat budget model for the ACW was constructed to test some of the above ideas. It is based on the following basic equation:

←

FIG. 4. (Uppermost) Surface velocities in the zonal direction. Eastward components of 0.03 m s^{-1} and greater are shaded. Contour interval is 0.02 m s^{-1}. (Lower nine panels) Lag sequence of the first mode of an EEOF analysis of sea surface temperature anomalies. The lag, in months, is shown in the box in the lower-right corner of each panel. Contour interval is 0.05 K; negative values are shaded.

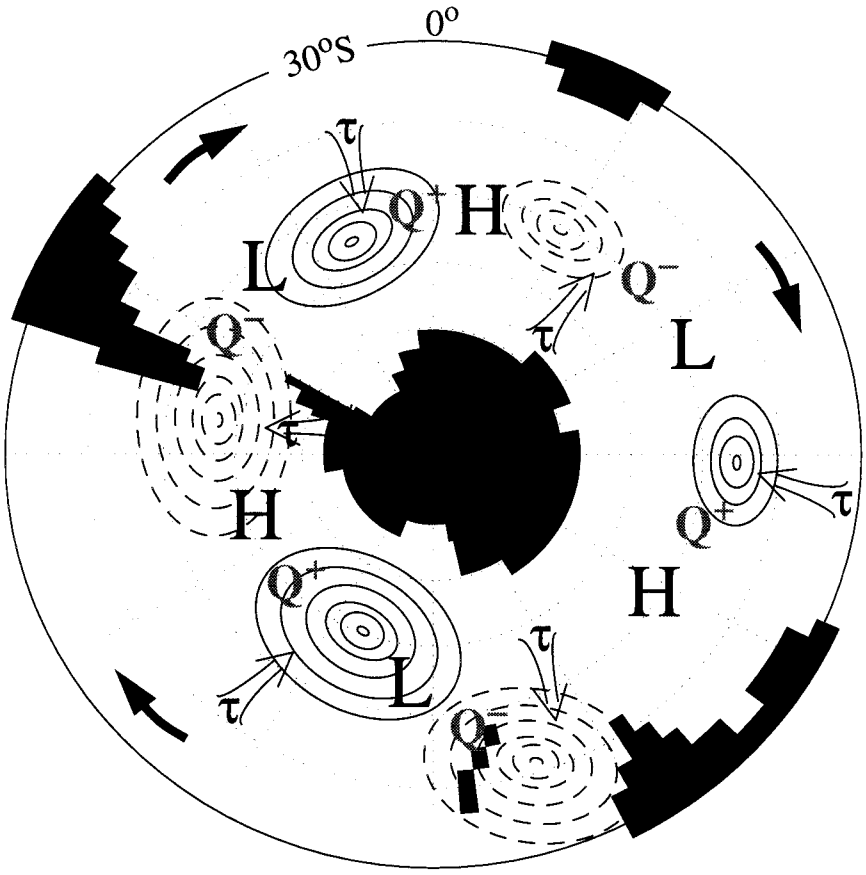

FIG. 5. Simplified schematic of spatial relationship between ACW components drawn for a specific phase. Contour lines depict sea surface temperature anomalies (negative contours are dashed), bold H and L represent the location of high and low pressure centers, Q^- and Q^+ indicate the position of upward and downward heat fluxes, and the meridional wind stress maxima are marked by τ. Heavy black arrows denote the general eastward propagation of SST anomalies while all the remaining components undergo a standing oscillation. This figure is crafted after that shown by White and Peterson (1996) for observations.

$$\frac{\partial}{\partial t}T(x, t) + u\frac{\partial}{\partial x}T(x, t) = Q(x, t),$$

where the sea surface temperature is denoted by T, the zonal speed of the background current in the advection term (second one on the left-hand side) is given by u, and Q represents the net local air–sea heat exchange. Assume a typical surface speed in the model (u = 16 yr $(360°)^{-1}$ = 0.04 m s^{-1} at 55°S) and let Q have a spatially *fixed* wavenumber 3 distribution together with a fluctuation period of 4 yr. Under these assumptions the model reproduced the basic CGCM results well as demonstrated in Fig. 9. The top panel shows the longitude–time diagram of the forcing term together with the surface speed of a tracer particle represented by the thin straight line. The bottom panel shows the corresponding Hovmoeller diagram for SST obtained from the above equation and the tracer particle is again represented by the thin straight line. The SST anomalies propagate at a phase speed of ~12 yr $(360°)^{-1}$ and are about 90° out of phase with the forcing pattern at any location with Q leading SST. Since the propagation speed of SSTs is larger than u, the question arises what other physics, apart from advection, are involved in this process. We believe that resonance effects are responsible for the difference. This will be discussed thoroughly in section 4.

Results very similar to the ones made in the previous paragraph are obtained when using a *propagating* signal in the forcing field of our simple model (Fig. 10), except

→

FIG. 6. Lag sequence of composite SST anomalies. Reference times are keyed to the maxima of the first principal component of EEOF analysis in Fig. 1 (threshold being one standard deviation). Contour interval is 0.05 K (negative contours are dashed). The 95% confidence levels according to a t test, based on dispersion of composite members, are indicated by light shading.

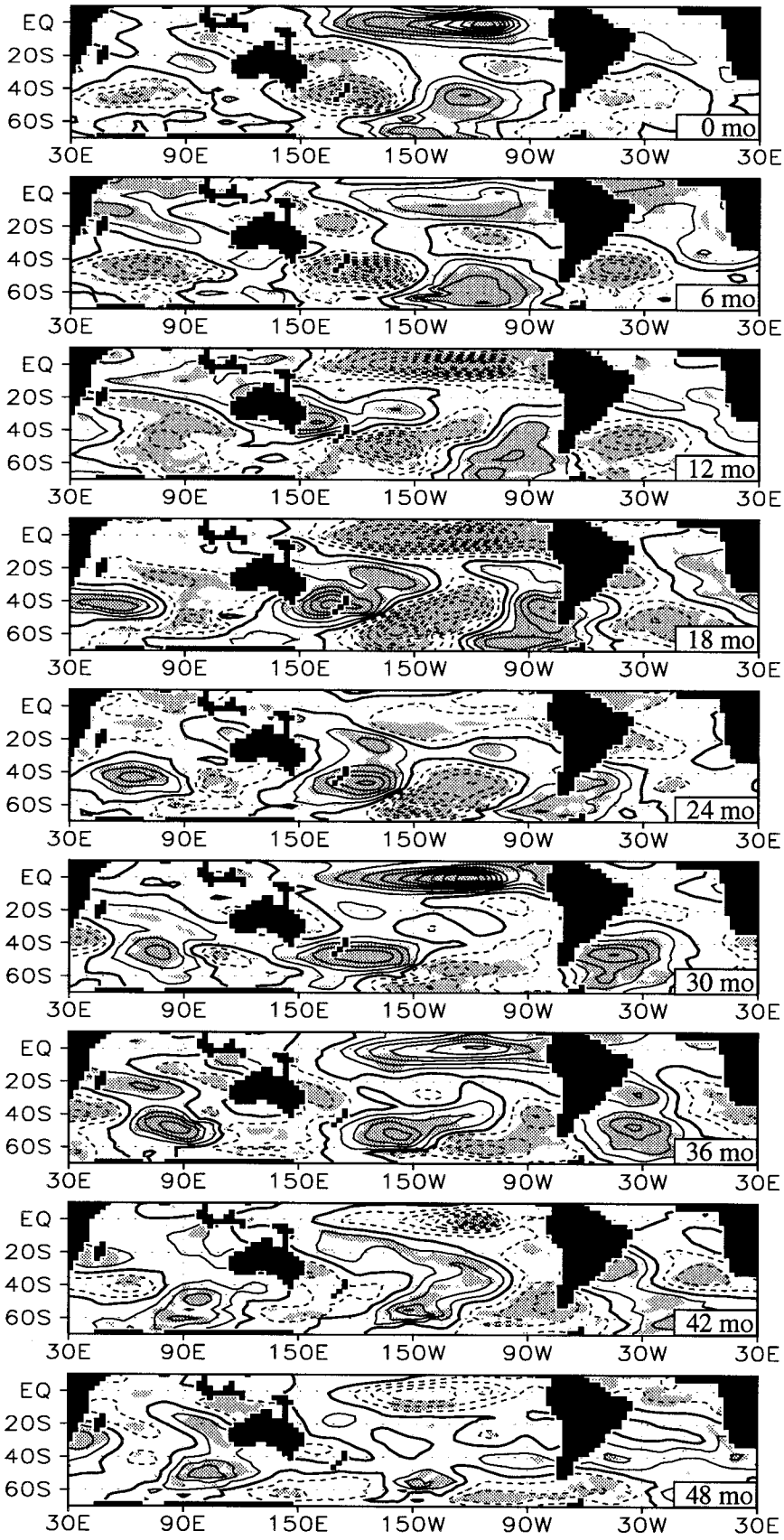

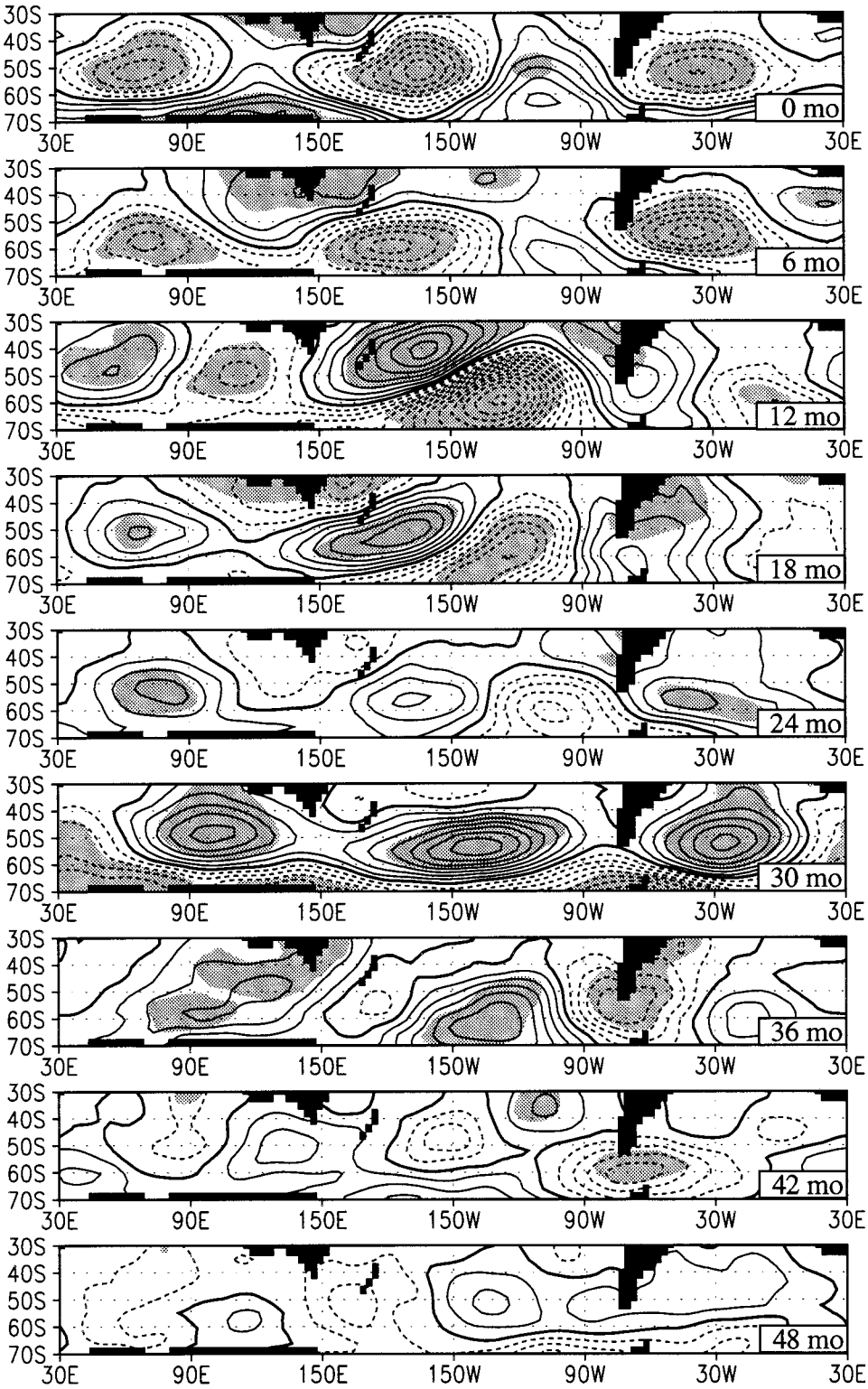

FIG. 7. As in Fig. 6 but for sea level pressure. Contour interval is 20 Pa (negative contours are dashed).

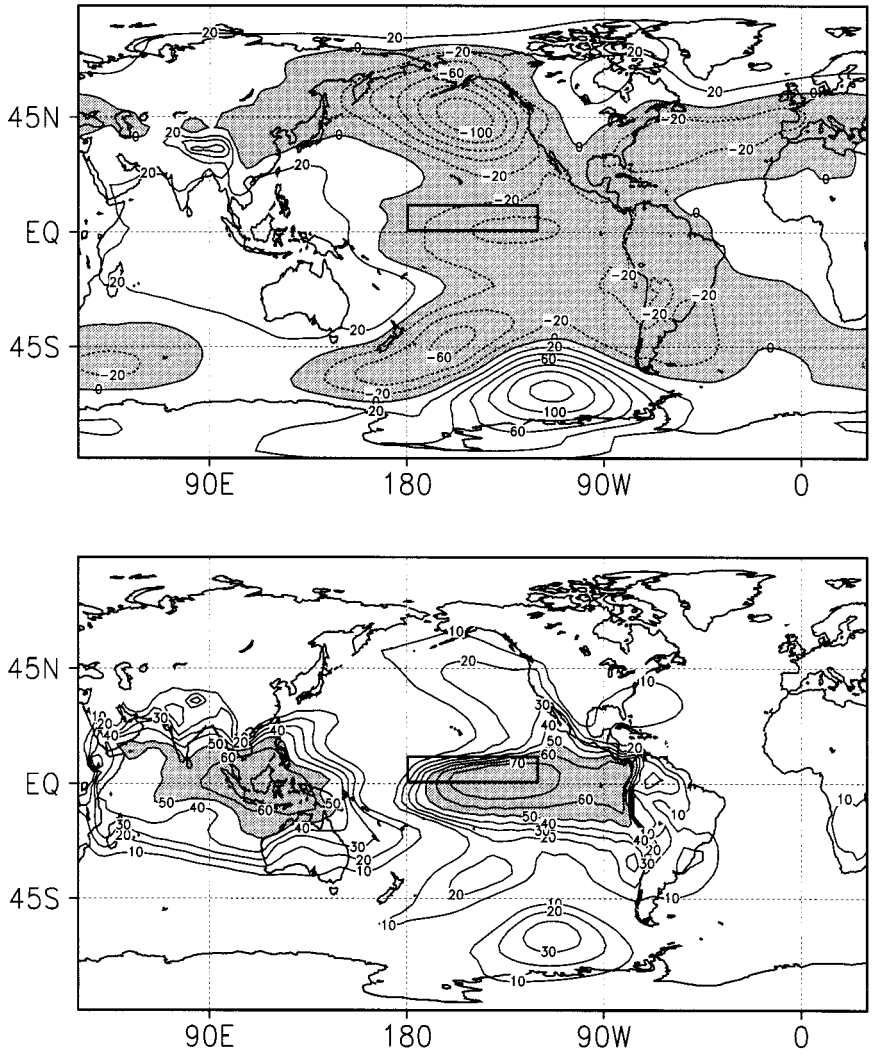

FIG. 8. Total precipitation averaged over the tropical central Pacific (0°–10°N, 180°–120°W) regressed upon gridpoint values of sea level pressure (top panel). Contour interval 20 Pa mm^{-1} day. Negative values are shaded. Box drawn with a heavy solid line represents index region of most influential precipitation. (Bottom) Skill (explained variance) of the linear regression model. Contour interval 10%; values larger than 50% are shaded.

for the higher amplitudes in SST. This result can be understood from the fact that the tracer particles in both settings see rather similar forcings along their paths through phase space. Hence, we see that even if the atmospheric ACW components in the obervations differ from those in the model with respect to propagation, they can still be part of the same phenomenon. Another implication of the simple model results is that phase locking is not a necessary condition for the existence of the ACW as implied by WP.

Further experimenting with our simplified model yielded that for both a standing wave and a propagating wave forcing pattern, the phase speed of the SST anomalies was largely tied to the wavenumber and frequency characteristics of Q. For instance, reducing its wavenumber from 3 (as in the CGCM) to 2 (as in the single realization in the observations and in 20% of the CGCM cases) leads to an acceleration of the SST anomalies from 12 yr $(360°)^{-1}$ to 8 yr $(360°)^{-1}$. This value is close to that found by WP for their wavenumber 2 case. Hence, the zonal wavenumber seems to be the critical element responsible for the differing timescales of the ACW between the CGCM and the ''real world.''

The speed of the underlying current was important in three ways. First, it determined the degree to which the energy spectrum of the SSTs was predominantly a propagating one. This dominance is ensured as long as the advection speed u is chosen from the interval 0.03–0.09 m s^{-1}. These numbers correspond to 0.5 and 1.5 times the ''resonance speed'' $u_{\text{res}} \equiv \omega k^{-1} = 0.06$ m s^{-1} at 55°S in Fig. 9. If $u \notin$ 0.03–0.09, then the SST spectrum is dominated by standing wave contributions. Sec-

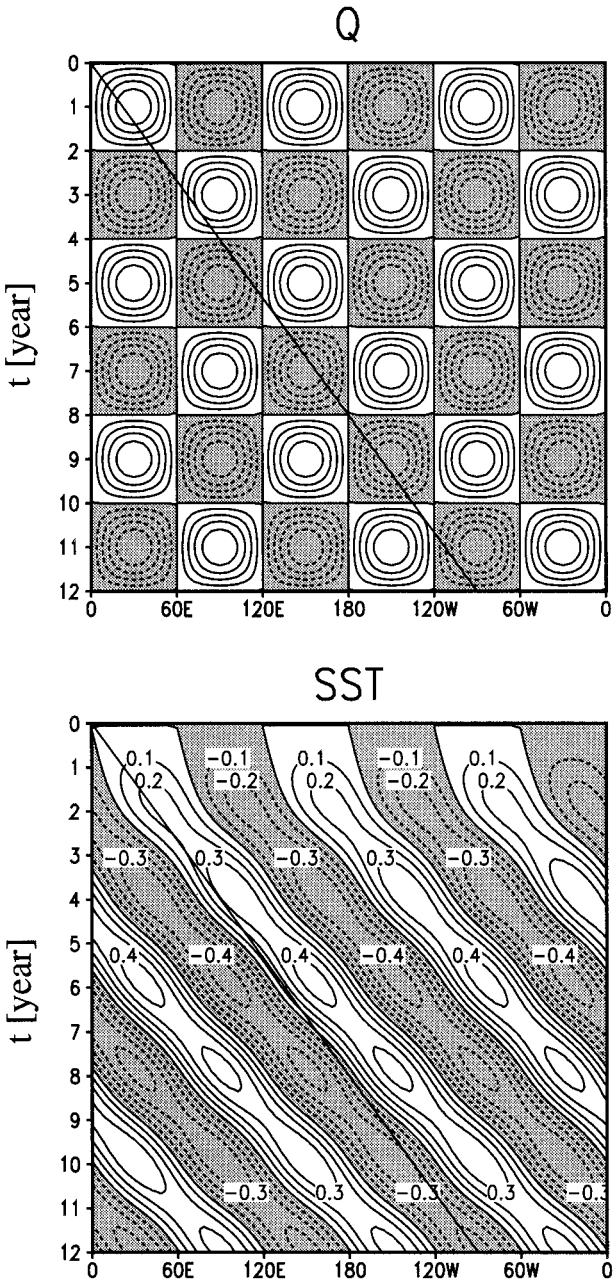

FIG. 9. Time–longitude sections taken from a simple ocean heat budget model. The forcing term Q in form of a standing oscillation (amplitude was set to 1 unit) and the resulting SST anomalies are given in the upper and lower panels, respectively. Contour interval is 0.2 for Q and 0.1 for SST. The thin line denotes a tracer particle chosen to represent the phase speed of the underlying current [16 yr $(360°)^{-1}$].

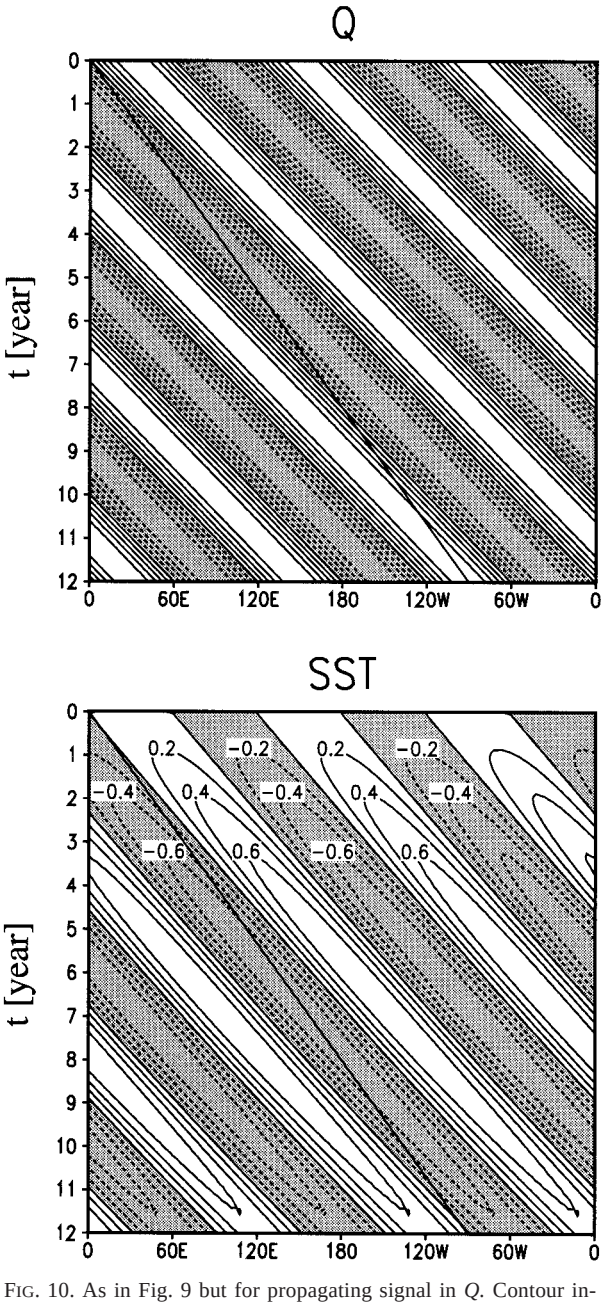

FIG. 10. As in Fig. 9 but for propagating signal in Q. Contour interval is 0.2 for Q and 0.2 for SST.

ond, the background currents influenced the amplitude A of the SST anomalies [$A \propto (u^2 - u_{\text{res}}^2)^{-1}$]. Third, they determined the relative phase relations between SST and Q. Accelerating the flow to the resonance speed of 0.06 m s^{-1} (when using Q of Figs. 9 or 10) brought the SST anomalies in phase with Q. Further increase of the speed to 0.08 m s^{-1} resulted again in a 90° out-of-phase relationship between Q and SST, but this time SST leading Q. Therefore, the specific phase relationship between SST and Q found in the CGCM (see Fig. 3d) can be explained in terms of an ACC being somewhat slower than the resonance speed determined by the atmospheric forcing pattern.

f. What determines the ACW timescale?

It is hypothesized by WP that the ACW is forced by ENSO via teleconnections. However, ENSOs in the

CGCM occur on average more often than the timescale of the ACW (Roeckner 1996; Bacher et al. 1996). How then can the ACW have a timescale of about 4 yr if it is forced by these tropical events? Based on the regression work noted above they may contribute somewhat to the ACW, but are not critical to its existence. And as stated above, a nonlinear analysis showed that the ACW was not a subharmonic of the model ENSO.

From the simplified model we learned that the timescale of all ACW components comes from the space–time characteristics of a specific atmospheric mode found in the southern midlatitudes. While one could argue that the preferred wavenumber 3 mass distribution is probably connected with the distribution of three continents and oceans, the origins of the roughly 4-yr period remain obscure.

4. Summary and discussion

The features of an ACW simulated by a coupled general circulation model are presented and compared with observations. Common features are the local timescale of about 4 yr, the temporal phase relationship between individual components along a latitude circle, and the eastward propagation of SST and sea ice anomalies. There also exist differences that, however, must be regarded both in the light of model deficiencies (ENSO timescale, resolution problems, etc.) and of the questionable data quality in the poorly sampled mid- to high latitudes of the Southern Hemisphere. Thus, improved and much longer observational datasets are required in the future in order to validate this model's and other coupled models' simulation of the ACW. The major differences we noted are as follows. There is a preferred zonal wavenumber 3 distribution of the ACW in the model as opposed to wavenumber 2 in the single realization from the observations. The anomalies of all observed variables propagate eastward at the same rate, that is, they are phase locked to each other, whereas in the model the atmospheric components are best represented by standing oscillations.

A mechanism responsible for the model ACW was suggested and tested with the help of a simplified model. The results obtained can best be summarized by drawing the following scenario. We start from a geographically fixed atmospheric forcing pattern of alternating heat sources and sinks that span the entire southern midlatitudes in a wavenumber 3 manner. The response to this forcing is a set of corresponding SST anomalies generated locally. The prevailing currents carry the entire SST pattern eastward at an average rate of 0.04 m s^{-1}, while the atmospheric anomalies simultaneously weaken and eventually reverse sign within 4 yr. This means the SST anomalies have to travel only to the next center of action before they get reenergized with the correct sign. Due to the almost equally spaced network of forcing centers around Antarctica, an anomaly, once created, has the chance to maintain itself against dissipation and make a complete circuit.

A closer look reveals, however, that SST and heat flux anomalies get temporally out of phase by some degree between two forcing centers due to the background flow being slightly too slow (up to 0.02 m s^{-1}) for full resonance at the location of the next downstream heat anomaly. Consequently, the SST anomalies do not remain completely intact while being advected, even if damping effects are neglected. This can be understood, for instance, from the view of a warm anomaly approaching a heat source. In our case, partial resonance means that its eastern and not its central parts are warmed the most when the downward fluxes are at a maximum. In other words, within the system of the ACC, there is always maximum SST warming tendency to the east of a warm anomaly. This physical process causes the SST anomalies to move eastward relative to the ACC and explains the discrepancy between the speed of the currents and the higher phase speed of the SSTs (0.06 m s^{-1}). Note that a similar mechanism for the apparent propagation of SST anomalies during an ENSO event was described in the literature (Barnett et al. 1991).

Another consequence of the superposition of advection and partial resonance processes is that not only the spatial scale but also the temporal scale of all ACW components is determined by the space–time characterstics of the atmospheric forcing pattern alone. This latter forcing can be associated with the PSA teleconnection, which is thought to be a natural atmospheric mode of the southern midlatitudes.

Giving detailed insight in the origins and temporal characterstics of the model's PSA pattern is beyond the scope of this paper. This question will be addressed in a subsequent study. Influences from ENSO, however, were shown to be marginal in the model's ACW. Another open question is whether the ACW both in the observations and in the model constitutes a truly coupled mode, that is, whether and how the SST anomalies feed back onto the atmospheric components.

Acknowledgments. The authors gratefully acknowledge the support of the German Ministry of Education and Research (BMBF) under Grant 07 VKV 01/1, the NOAA-sponsored SIO/Lamont Consortium (NOAA NA47GPO188), DOE's CHAMMP effort (DE-FG03-91-ER61215), and the National Science Foundation (NSF ATM-93-14495). We are grateful to Warren White who shared with us the results of his observational studies that provided the motivation for this work. Also, we would like to thank Niklas Schneider and Mojib Latif for valuable comments. Special thanks to Josef Oberhuber for numerous discussions and to Andreas Bacher who did all the coupling work and provided the filter routines. Finally, the considered and spurring reviewers' suggestions had a substantial impact on this article. We thank them for their effort.

REFERENCES

Bacher, A., J. M. Oberhuber, and E. Roeckner, 1996: ENSO dynamics and seasonal cycle in the tropical Pacific as simulated by the ECHAM4/OPYC3 coupled general circulation model. Max Planck Institute for Meteorology Rep. No. 199, 29 pp. [Available from Max-Planck Institute for Meteorology, Bundesstrasse 55, D-20146 Hamburg, Germany.]

Barnett, T. P., 1988: Variations in near-global sea level pressure: Another view. *J. Climate,* **1,** 225–230.

——, 1991: The interaction of multiple time scales in the tropical climate system. *J. Climate,* **4,** 269–285.

——, E. Kirk, M. Latif, and E. Roeckner, 1991: On ENSO physics. *J. Climate,* **4,** 487–515.

Horel, J. D., and J. M. Wallace, 1981: Planetary-scale atmospheric phenomena associated with the Southern Oscillation. *Mon. Wea. Rev.,* **109,** 813–829.

Karoly, D. J., 1989: Southern Hemisphere circulation features associated with El Niño–Southern Oscillation events. *J. Climate,* **2,** 1239–1252.

Mo, K. C., and G. H. White, 1985: Teleconnections in the Southern Hemisphere. *Mon. Wea. Rev.,* **113,** 22–37.

Oberhuber, J. M., 1993a: Simulation of the Atlantic circulation with a coupled sea ice–mixed layer–isopycnal general circulation model. Part I: Model description. *J. Phys. Oceanogr.,* **23,** 808–829.

——, 1993b: The OPYC ocean general circulation model. Deutsches Klimarechenzentrum GmbH Tech. Rep. 7, 130 pp. [Available from DKRZ, Bundesstrasse 55, D-20146 Hamburg, Germany.]

Read, J. F., and R. T. Pollard, 1993: Structure and transport of the Antarctic Circumpolar current and Agulhas return current at 40°E. *J. Geophys. Res.,* **98,** 12 281–12 295.

Roeckner, E., J. M. Oberhuber, A. Bacher, M. Christoph, and I. Kirchner, 1996: ENSO variability and atmospheric response in a global coupled atmosphere–ocean GCM. *Climate Dyn.,* **12,** 737–754.

Weare, B. C., and J. S. Nasstrom, 1982: Examples of extended empirical orthogonal function analyses. *Mon. Wea. Rev.,* **110,** 481–485.

White, W. B., and R. G. Peterson, 1996: An Antarctic circumpolar wave in the surface pressure, wind, temperature and sea-ice extent. *Nature,* **380,** 699–702.